Microscopic partition of pressure and elastic constants in CdTe polymorphs

T. Ouahrani[a,b], R. Franco[c], J. M. Menéndez[c], M. Marqués[c], J. M. Recio[c,*]

[a] *Laboratoire de Physique Théorique, Tlemcen University, 13000 Tlemcen, Algeria*
[b] *École Préparatoire en Sciences et Techniques, 13000 Tlemcen, Algeria*
[c] *MALTA Team and Departamento de Química Física y Analítica, Universidad de Oviedo, E-33006 Oviedo, Spain*

Abstract

In the frame of density functional theory, first principles calculations were carried out to determine pressure stability ranges of zinc-blende (B3), cinnabar (Cinn), rock-salt (B1), orthorhombic (*Cmcm*), and cesium chloride (B2) phases of CdTe. In agreement with experimental observations, we found a B3 → Cinn → B1 → *Cmcm* pressure-induced sequence, and predict the B2 phase as a potential high pressure polymorph. The equations of state of all these polymorphs and the components of the elasticity tensor of the B3 phase at zero pressure were determined and microscopically analyzed in terms of atomic contributions. The concept of local pressure allows for quantifying differences in the role played by Cd and Te as regards the compressibility of CdTe phases, and suggests the existence of a general behavior under pressure for binary II-VI semiconductors.

Keywords: atomic scale structure, high-pressure, computer simulations, semiconductors, phase transitions

*Corresponding author: jmrecio@uniovi.es

1. Introduction

CdTe is a II-VI semiconductor compound belonging to the cadmium chalcogenide crystal family. This is a group of important materials for the development of various modern technologies of solid state devices such as solar cells [1]. In particular, CdTe has an ideal direct band gap energy of 1.45 eV and a high absorption coefficient, which makes a very thin layer of this material sufficient for a high energy conversion efficiency [2]. Along with the electronic properties, the mechanical behavior of CdTe has also been the subject of many experimental studies, including pressure effects using Raman spectroscopy [3] and transport measurements [4]. Special attention has been paid to the structural changes of this compound in connection with the reconstructive phase transition sequence exhibited by other binary chalcogenides at high pressure [3, 4, 5, 6].

Using angle-dispersive techniques and image–plate detectors, Nelmes *et al.* [6] rather unexpectedly found that CdTe undergoes a rich polymorphism under applied high pressure. They found the transition sequence zinc-blende (B3) $\rightarrow$ cinnabar (Cinn) $\rightarrow$ rock-salt (B1) $\rightarrow$ $Cmcm$ with transition pressures of 3.5 GPa (B3–Cinn), 3.8 GPa (Cinn–B1), and 10 GPa (B1–$Cmcm$), respectively. According to this work, the cinnabar phase of CdTe only exists in a narrow pressure range around 3.5 GPa, which explained why it had not been found in previous experiments. This polymorphic sequence is now well established and clarifies controversy regarding the existence of the cinnabar phase for CdTe (see for example Ref. [7]). From the theoretical side, only a few works have accurately simulated the correct sequence of pressure-induced phase transitions for CdTe [8, 9, 10]. Moreover, there is still a lack of fun-

damental understanding of several aspects regarding the role played by the atomic constituents of these binary semiconductors in their compressibility and in the corresponding transition pressures.

Though it is clear according to previous works (see for example Ref. [11]), that macroscopic compressibility is one of the key parameters linked to polymorphic sequences, phase stability is ultimately determined by the crystalline bonding network, and hence by the valence electrons of the particular atomic constituents of the solid. To understand the complex factors connecting stability and equation of state (EOS) parameters of compounds, one appealing route is to decompose macroscopic observable properties in terms of local contributions, and more specifically, of meaningful chemical entities as the atomic constituents of the materials. This is also of critical importance in materials design and earth studies where a decomposition of compressibility as a sum of atomic-like contributions allows one to rationalize trends and to guide materials synthesis [12, 13]. A formalism that is best suited along this line relies on the rigorous quantum-mechanical analysis of the topology of the crystalline electron density provided by the *Atoms in Molecules* theory (AIM) [14]. With this formalism, we have shown in previous works how the partition of static thermodynamic properties like the bulk modulus can be used, for example, to explain the uniform behavior of a number of cubic oxide spinels under pressure [12, 13]. Greater fractional occupation of the oxide anion sublattice and the greater compressibility of these anions (around 200 GPa) are the parameters that control the response to hydrostatic pressure of all of these oxide spinels. More recently, Otero-de-la-Roza and Luaña also proposed a feasible method for partitioning the non-isotropic elastic compo-

nents into atomic contributions by means of the AIM formalism [15].

Further insight into the behavior of solids under pressure can be given using a new definition of local pressure: the resistance exerted by an atom against volume reduction when pressure is applied [16]. The way several ZnX (X: S, Se, Te) polymorphs nicely follow a common trend when these atomic-like (Zn and X) pressures are considered has been recently illustrated [16]. An extension of our previous calculations to other polymorphs with a different cation is desirable to test the performance of this new concept in the binary II-VI semiconductor family.

In this contribution, our main goal is to clearly identify the role played by Cd and Te in the polymorphic sequence exhibited by CdTe under hydrostatic pressure. To this end, we analyse the partition of the unit cell volume of all observed CdTe polymorphs (plus the hypothetical B2 phase) into well-defined, disjoint, and space-filling regions (basins) associated with these atomic constituents, applying the AIM formalism to the crystalline wave functions obtained after extensive first principles computations. Quantitative data of the pressure effects on the calculated atomic-like basins is obtained through careful equation of state fittings. This information is used to evaluate local pressures, compressibilities, and elastic constants for Cd and Te. A comparison with our previous results in other binary chalcogenides is also performed to check if our findings are general for this crystal family.

The rest of the paper is organized as follows. In Section 2, the computational modeling is presented, giving details on the electronic structure calculations, EOS fitting procedure, the scheme for the evaluation of the components of the elasticity tensor, and a brief presentation of the topological

partition formalism applied to the crystalline electron density. Results and discussion in Section 3 are split into two subsections. The first one presents bulk properties: EOS parameters, the phase transition diagram and elastic constants. Comparison with available experimental data and results from other theoretical calculations is included. The second one deals with the microscopic partitioning of macroscopic properties focusing on the common trend of atomic pressures for all polymorphs of the binary II-VI compounds studied so far. A brief summary and the main conclusions are gathered in Section 4.

2. Computational Modeling

Unlike simple theoretical calculations for cubic unit cell structures, some of the phases belonging to the pressure-induced polymorphic sequence of CdTe involve several structural parameters to optimize, and not only total energy, but also atomic forces and stress tensor components have to be computed. We have calculated the crystalline energy (E) at different volumes of the unit cell (V) for the following polymorphs: wurtzite (B4), zinc blende (B3), cinnabar (Cinn), rock-salt (B1), orthorhombic ($Cmcm$), and cesium chloride (B2); E and V always refer to one CdTe formula unit. B3 ($F\bar{4}3m$), B1 ($Fm3m$), and B2 ($Pm\bar{3}m$) are cubic structures and only the lattice parameter a has to be determined. B4 ($P6_3mc$) and cinnabar ($P3_121$) are hexagonal phases and both a and c lattice parameters are needed to determine the unit cell size. In addition, the z coordinate of Te (usually referred to as u) for the B4 structure, and the x coordinate of Cd and Te non-equivalent atoms (usually referred to as u and v, respectively) for the cinnabar structure

need to be evaluated. Finally, the orthorhombic ($Cmcm$) unit cell is completely defined with the unit cell parameters a, b, and c, and the y coordinate of Cd and Te non-equivalent atoms.

First-principles total-energy calculations at selected unit-cell volumes of all the structures were performed under the formalism of the density functional theory with the `ABINIT` code [17]. We used the Perdew-Burke-Ernzerhof (PBE) exchange-correlation functional [18] and norm-conserving Troullier-Martins pseudopotentials [19] with 12 and 6 valence electrons for Cd an Te, respectively. Due to the existence of energetically competitive structures, we ensured that the absolute total energies converged to 10^{-6} hartree/atom. To this end, we used 8×8s×8, 6×6×8, and 4×8×6 Monkhorst-Pack meshes [20] for the cubic, tetragonal and hexagonal, and orthorhombic lattices, respectively and the plane-wave cutoff energy was set to 60 hartrees. Optimization of the unit cell geometry and atomic positions at each volume was performed via a Broyden-Fletcher-Goldfarb-Shanno (BFGS) minimization (see Ref. [17]) of the total energy using the Hellmann-Feynman forces on the atoms and the stresses on the unit cell. During the calculations, relaxations of both the internal structural parameters and the cell shape were included. The structural relaxation was performed until the residual forces and stresses were less than 5×10^{-5} hartree/bohr and 5×10^{-7} hartree/bohr^3, respectively. The chosen computational parameters (cutoff energy, k-point meshes, force tolerance, etc.) guarantee an accurate determination of the polymorphic sequence and the corresponding structural and energetical properties.

For each polymorph, the equilibrium volume V_0, the bulk modulus B_0, and its first pressure derivative B_0' (the 0 subscript meaning that all these

quantities were evaluated at zero pressure) are then obtained by introducing the corresponding energy-volume (per unit formula) (E,V) points as input to the GIBBS code [21]. This is a well-tested computational code that implements a combined statistical numerical analysis with well-known analytical EOS such as those of Vinet, Birch, Murnaghan, etc. (see Ref. [21] and references therein). The standard strategy for the evaluation of the relative stability of high-pressure phases at static conditions (zero temperature and zero point vibrational contributions neglected) is based upon the examination of enthalpy ($H = E + pV$) as a function of pressure (p) for different phases. This task is also performed with the GIBBS code.

Dynamical stability of high pressure cubic phases was also analyzed after the determination of the phonon dispersion curves for the B1 and B2 phases. We computed the interatomic force constants by Fourier transformation of the dynamical matrices computed on 4×4×4 regular q-point grids. Due to the metallic character of the high pressure phases of CdTe, the calculations of the initial wave functions were performed on 16×16×16 k-point meshes and including a cold smearing of 0.01 hartree. Whereas this parameter is relevant to the evaluation of the phonon dispersion curves, we have checked that it does not affect the energy-volume curves.

Concerning the calculation of the components of the elasticity tensor, the subject was a matter of debate in the last decades (see for example Ref. [22]). One elegant scheme, involving first derivatives of the stress and not second derivatives of the energy, has been proposed by Le-Page and Saxe [23], and illustrated by Hector *et al.* and others including pressure effects (see for example [24, 25, 26, 27]). For the evaluation of these components just at

zero pressure and in the cubic structure of the B3 phase of CdTe, we can carry out a simple procedure described in Ref. [15] and detailed as follows. Within the elastic domain of the crystal (*i.e.* infinitesimal deformations with respect to the equilibrium configuration), stress (τ) and strain (ϵ) are related by linear transformations:

$$\tau_{ij} = \sum_{kl} c_{ij,kl}\epsilon_{kl} \quad \text{and} \quad \epsilon_{ij} = \sum_{kl} s_{ij,kl}\tau_{kl}, \tag{1}$$

where the indexes run over the three (x,y,z) cartesian coordinates and $c_{ij,kl}$ and $s_{ij,kl}$ are the elastic constant and the elastic compliance components, respectively. The bidimensional τ and ϵ tensors can be transformed into one index of vectors using the Voigt [28] notation:

$$[\tau_{11}, \tau_{22}, \tau_{33}, \tau_{23}, \tau_{31}, \tau_{12}] \Rightarrow [\tau_1, \tau_2, \tau_3, \tau_4, \tau_5, \tau_6] \tag{2}$$

and

$$[\epsilon_{11}, \epsilon_{22}, \epsilon_{33}, \epsilon_{23}, \epsilon_{31}, \epsilon_{12}] \Rightarrow [\epsilon_1, \epsilon_2, \epsilon_3, \epsilon_4, \epsilon_5, \epsilon_6]. \tag{3}$$

Under the Voigt notation, and in the limit of infinitesimal deformations, $c_{ij,kl}$ and $s_{ij,kl}$ can be expressed with just two indexes as follows:

$$c_{ij} = \left(\frac{\partial \tau_i}{\partial \epsilon_j}\right)_{\boldsymbol{\epsilon'},\mathbf{0}} \quad \text{and} \quad s_{ij} = \left(\frac{\partial \epsilon_i}{\partial \tau_j}\right)_{\boldsymbol{\tau'},\mathbf{0}}, \tag{4}$$

where primes and the zero subscripts indicate, respectively, that all other strains (stresses) are null and the derivatives are evaluated at the equilibrium geometry.

Alternatively, in terms of the total volume, Eq. 4 becomes:

$$c_{ij} = \left(\frac{\partial \tau_i}{\partial \varepsilon_j}\right)_{\varepsilon',0} = \left(\frac{\partial \tau_i}{\partial V}\frac{\partial V}{\partial \varepsilon_j}\right)_{\varepsilon',0}. \tag{5}$$

These equations will be further exploited below. Now, for the practical calculation of the elastic constants, we recall the following expression for the elastic energy of the crystal (see Ref. [15]):

$$\phi = \frac{E - E_0}{V_0} = \frac{1}{2} \sum_{ij,kl} c_{ijkl} \epsilon_{ij} \epsilon_{kl}, \tag{6}$$

where V_0 and E_0 are the equilibrium cell volume and energy, respectively.

In a cubic system, there are only three independent elastic constants (compliances): $c_{11}(s_{11})$, $c_{12}(s_{12})$, and $c_{44}(s_{44})$. Using Eq. 6, the elastic constants of the B3 cubic phase of CdTe have been obtained as follows. At eleven values for each of the strains ϵ_1, ϵ_2 and ϵ_4, ranging respectively from -0.04 to 0.04, from -0.01 to 0.01, and from -0.06 to 0.06, we have calculated the elastic energy of the corresponding unit cell including optimization of all the free structural parameters that are compatible with the deformations.

In addition, we have carried out a microscopic analysis of the topology of the electron density of all the CdTe polymorphs using Bader's AIM formalism and the CRITIC program [29]. To this end, calculated equilibrium geometries have been considered. The AIM formalism allows for a chemical characterization of a crystalline solid in terms of critical points where the gradient of the electron density, ρ, is zero. Zones of charge depletion and charge accumulation are associated with low values of ρ and positive Laplacians and with high values of ρ and negative Laplacians, respectively. The unit cell volume can be divided into well-defined, disjoint, and space-filling regions, called basins, that are surrounded by a surface where the flux of the gradient of the electron density is null. Thanks to the CRITIC code [29], it is possible to perform an unequivocal evaluation of the atomic volumes of Cd

and Te in all the polymorphs at different pressures, thus providing the raw data for the calculation of atomic-like equations of state.

3. Results and Discussion

3.1. Bulk properties

3.1.1. Total Energy and Equation of State

We start presenting the results obtained from total energy minimizations with respect to all the unit cell parameters and internal coordinates at selected sets of volumes for the six polymorphs of CdTe studied in this work. This step is mandatory if we look for a microscopic partition of pressure. All the calculated (E,V) points can be described by means of smooth curves as displayed in Fig. 1. From the corresponding data sets, the EOS parameters (V_0, B_0, B_0') and the pressure-volume (p-V) curves of all the polymorphs have been calculated with the GIBBS code [21]. We have completed extensive numerical analyses in order to secure stability of the computed zero pressure equilibrium values gathered in Table 1 against variations in sampling points and fitting schemes.

According to our static calculations, B3 is predicted to be the stable phase at zero pressure. As expected from their similar atomic environments, wurtzite (B4) and B3 are almost degenerated showing a difference in energy (ΔE_0) close to the accuracy of the calculation (10^{-5} hartree). In addition, ΔE_0 (energy of each polymorph at equilibrium referred to the B3 phase) and V_0 values (see Table 1) follow monotonous trends suggesting the observed pressure-induced polymorphic sequence: B3 $\rightarrow$ Cinn $\rightarrow$ B1 $\rightarrow$ $Cmcmn$, with a prediction of B2 for a potential phase at very high pressures. This issue will

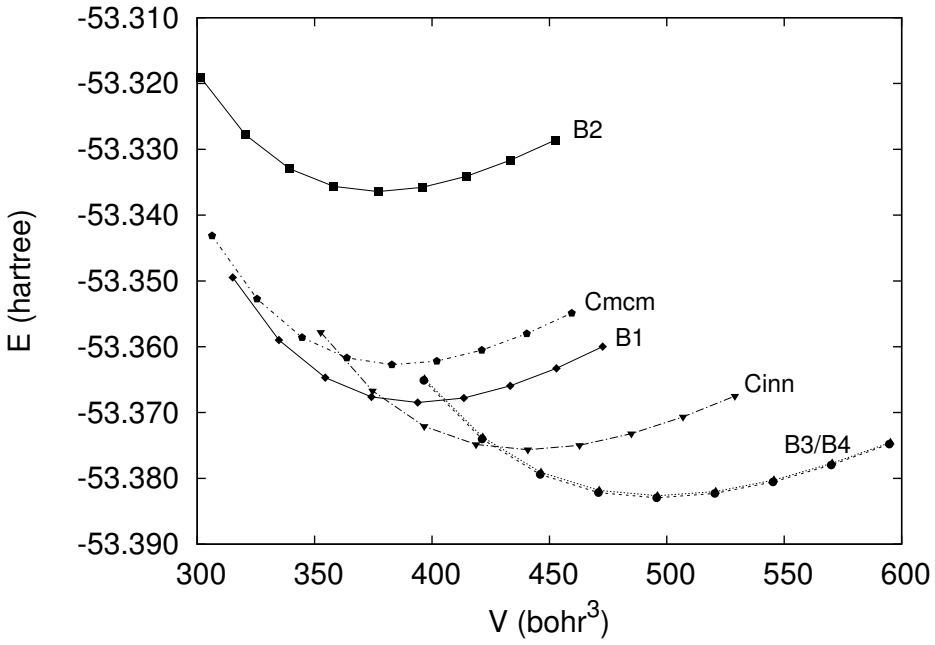

Figure 1: Calculated total energy versus volume per formula unit for several polymorphs of CdTe

be discussed below. As regards the comparison with available experimental data at room temperature, it is to be noticed that theory yields greater volumes and lower bulk moduli, with discrepancies that are a little bit larger than expected for GGA-type calculations. Notice, for example, that our B_0 value for the ambient conditions stable B3 phase (34.5 GPa) lies within the wide range of values quoted in Ref. [30] (from 13.3 GPa to 66 GPa) that includes up to eighteen theoretical and experimental data. One of the values quoted at 4 K (44.5 GPa) is close to the one quoted from X-ray diffraction meassurements at room T (42 GPa), illustrating minor effects of temperature on B_0 in this T range. However, it is important to highlight that our focus

Table 1: Calculated EOS parameters of CdTe polymorphs. ΔE_0 refers to the minimum energy of a given polymorph with respect to the B3 phase. For each property, the first row lists calculated values in this work and, when present, the second row lists data from experiments at room temperature or from other static calculations when experiments are not available. Unit cell parameters in Å, V_0 in Å^3, B_0 in GPa and ΔE_0 in hartree.

	B4	B3	Cinnabar	B1	*Cmcm*	B2
a, b, c	4.694, 7.699	6.647	4.641, 10.49	6.158	6.155, 6.006, 5.271	3.821
	4.57[a], 7.49[a]	6.48[b]	4.292[c],10.235[c]	5.93[c]	5.573[d], 5.960[d], 5.284[d]	3.788[e]
u, v	0.3798		0.50, 0.83		0.16,0.63	
			0.641,0.564[c]		0.18[d],0.65[d]	
V_0	73.53	73.46	65.31	58.38	57.08	55.89
B_0	34.3	34.5	38.8	45.7	45.7	43.6
	42.1[f]	42[g]	32[g], 51.7[h]	69[g]	67[h]	45.9[h]
B'	4.78	4.80	4.85	4.98	4.94	4.84
ΔE_0	0.0003	0.00	0.0073	0.0145	0.0202	0.0465

[a]Ref. [31], [b]ref. [32], [c]at 3.6 GPa, quoted in Ref. [10], [d]at 18.6 GPa, quoted in Ref. [10], [e]calculated, Ref. [10], [f]ref. [33], [g]quoted in Ref. [30], [h]calculated, quoted in Ref. [10].

is on the atomic contributions along the polymorphic sequence as pressure is applied. Fortunately, these differences are not expected to affect the final results of our microscopic analysis.

3.1.2. Phase Diagram

Our calculated E-V and p-V curves are the main source to evaluate how the enthalpy, H, evolves as pressure is applied. In order to determine all possible pressure-induced phase transitions, we have evaluated how the difference

between the enthalpies of all pairs of structures changes with pressure, and have determined the transition pressure (p_t) applying the equilibrium condition ΔH=0. Results are displayed in Fig. 3. In spite of the number of curves plotted, we believe that it is worth exploring all of the possibilities, although only the most important results will be summarized here.

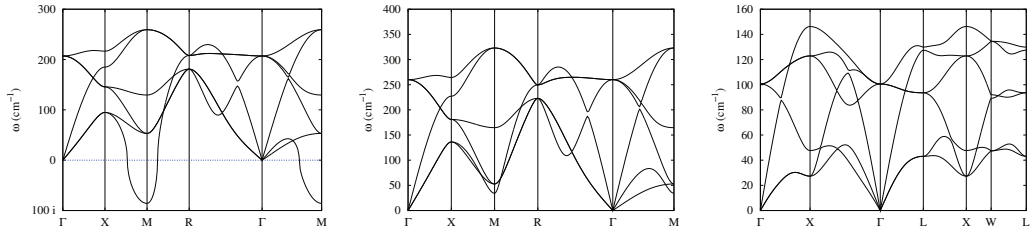

Figure 2: Calculated phonon dispersion curves for the B2 phase at 71 GPa (left) and 123 GPa (middle), and for the B1 phase at 5 GPa (right)

If we list the computed stable phases (lowest H) as pressure is applied, we find the same polymorphic sequence as experimentally observed (in brackets calculated p_t values): B3 $\rightarrow$ Cinn (4.4 GPa), Cinn $\rightarrow$ B1 (5.1 GPa), and B1 $\rightarrow$ $Cmcm$ (22 GPa). Comparison with experimental p_t values at room temperature [6] shows some discrepancies (3.5 GPa, 3.8 GPa, and 10 GPa are the observed transition pressures, though coexistence of phases within pressure ranges of few GPa are detected and should also be considered) that are in part due to our GGA level of calculation. Other phase transition properties show the correct trend and quantitative agreement with previous theoretical calculations, although it is difficult to make a direct comparison with available experimental data due to the different definitions and the disparity of reported values. For example, our calculated (in brackets, theoretical results from Ref. [8]) volume collapses with respect to the transition volume of the

corresponding low pressure phase along the above transition sequence are 10.3% (13.1%), 9.5% (7.5%), and 2.2% (1.8%). The experimental values at room temperature for the same transitions quoted in Ref. [8] are 14.3%, 3.7% and a value lower than 1%.

In addition, the $Cmcm \rightarrow$ B2 phase transition is predicted at a pressure above 70 GPa (not displayed in Fig. 3). In order to further validate the dynamical stability of the B2 phase predicted from our static calculations, we have determined phonon dispersion curves for this high-pressure structure. Although the B2 phase presents an imaginary frequency in the vicinity of the M point at 71 GPa (Fig. 2 (left)), it is metastable (positive frequencies at Γ). Moreover, the imaginary frequency disappears at pressures close to 110 GPa and the phase becomes fully dynamically stable (Fig. 2 (middle)). Additionally, phonon dispersion curves for the B1 phase were determined. The abscence of imaginary frequencies in the whole Brillouin zone for the B1 phase at 5 GPa, within its experimental range of existence, informs on its dynamical stability (Fig. 2 (right)).

It is even more important to highlight that the B3 $\rightarrow$ B1 and B3 $\rightarrow Cmcm$ phase transitions are computed at 4.8 GPa and 6.2 GPa, respectively, which is very close to the B3 $\rightarrow$ Cinn value of p_t (see inset of Fig. 3). Therefore, attention should be paid when comparing the calculated (thermodynamic) polymorphic sequence with that observed experimentally. A number of factors involved in the kinetics of these transformations (defects, hysteresis, thermal barriers, etc.) could favor, for example, the transition from the B3 phase into the B1 phase, thus masking the cinnabar phase. To this regard, it is interesting to note that Martínez-García *et al.* found in their energy

dispersive X-ray experiments that, as temperature increases (above 773 K), B3 transforms directly to B1, thus skipping the cinnabar phase [7]. We are currently working on the definition of a transition path connecting B3, cinnabar, and B1 phases that will lead to the evaluation of the corresponding energy barriers following a martensitic-like approach as we did, for example, for the zircon-scheelite transition in $ZrSiO_4$ [34]. Similarly, other transformations, as the Cinn $\rightarrow$ *Cmcm* calculated at 8.1 GPa, might prevent the occurrence of the B1 phase, though, as far as we know, this situation has not been previously reported. To complete this discussion, we should point out that (high) temperature could play an important role in the evaluation of these phase boundaries. The quasiharmonic approximation constitutes the computational strategy to follow as illustrated by Wrobel *et al.* [35] or Otero-de-la-Roza and Luaña [36], though its application is out of the scope and goals of this work.

3.1.3. Elastic Constants

As an example, Fig. 4 illustrates how the elastic energy of the B3 unit cell departures from its equilibrium value (which is taken as 0 for reference) as the cell is deformed following the unidimensional strains ϵ_1 and ϵ_4 involved, respectively, in the elastic constants c_{11} and c_{44}. Our GGA calculated values for the elastic constants are compared with earlier experimental results [37] at room temperature in Table 2. The discrepancy between our results and those experimentally obtained is not higher than 20% for c_{11} and c_{12}, whereas it is about 10% for c_{44}. In lanthanum-magnesium phases, a comprehensive study comparing standard functionals with a critical analysis of their performance under static and temperature conditions show that the calculated compone-

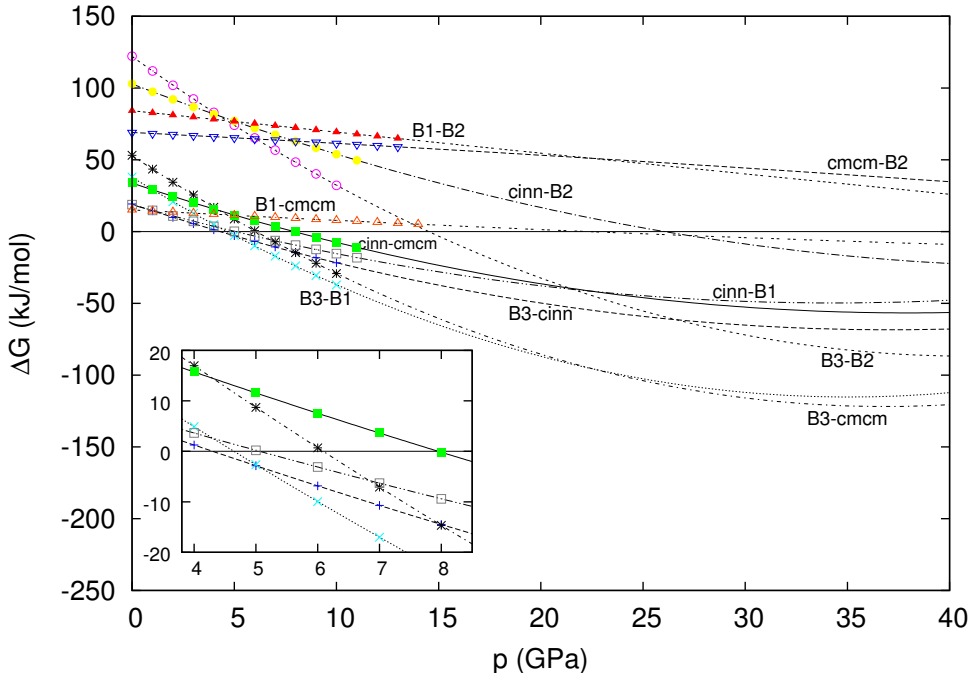

Figure 3: Calculated ΔG energies for all phase transitions involving CdTe polymorphs. The inset enhances a relevant pressure range with competitive phase transitions. Pressure in GPa. Energy in kJ/mol.

nents of the elasticity tensor are not systematically affected by the type of functional when comparing with the corresponding experimental values [35]. Additionaly, it is to be noticed that the mechanical stability conditions involving the elastic constants in cubic crystals ($c_{11} - c_{12} \geq 0$, $c_{11} + 2c_{12} \geq 0$, and $c_{44} \geq 0$) are seen to be satisfied in our calculations (see Table 2).

In order to further test the consistency of our calculations, Table 2 also lists the B_0 value obtained from the EOS fitting in the previous section (last column) and the one derived from the elastic constants relationship in cubic crystals: $B_{0,\mathrm{el}}=\frac{1}{3}\,(c_{11} + 2c_{12})$. A very good agreement is found between these

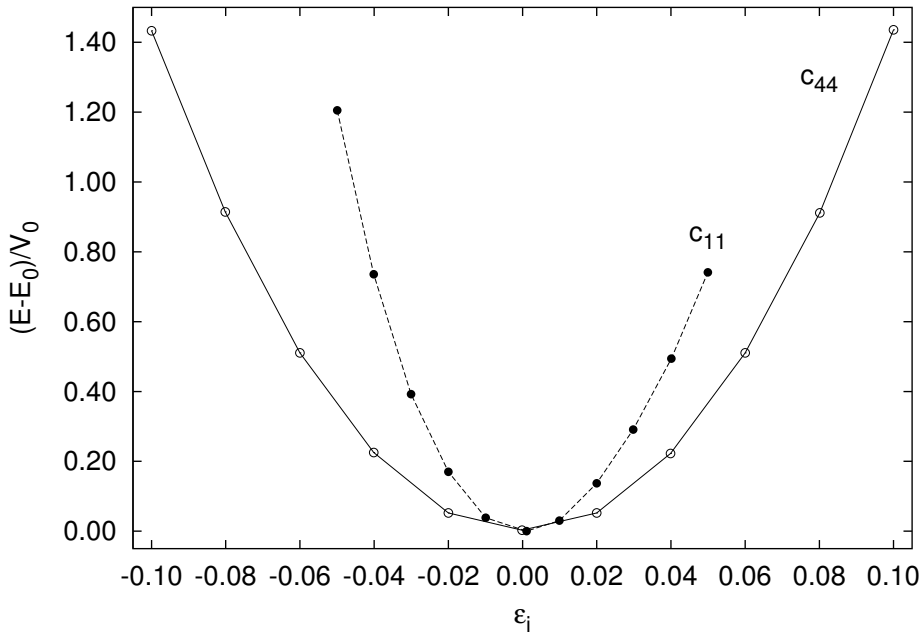

Figure 4: Elastic energy, $\phi(\epsilon_i)\times 10^5$ in units of hartree/bohr^3, along strains ϵ_1 and ϵ_4 involved, respectively, in the evaluation of the elastic constants c_{11} and c_{44}.

two values (B_0=34.5 GPa, $B_{0,\mathrm{el}}$=34.7). Given the different origin and fitting schemes used in their evaluation, this result provides further reliability to our computational procedures.

3.2. Local Properties

3.2.1. Local Pressure

Once the observed behavior of CdTe under pressure has been computationally simulated, we moved on to the microscopic interpretation in terms of atomic-like contributions. The unit cell volumes of the CdTe polymorphs have been topologically partitioned into Cd and Te basins, V_{Cd} and V_{Te}, for all the computed (E,V) points by means of the AIM formalism. As a result,

	f	c_{11}	c_{12}	c_{44}	$B_{0,\mathrm{el}}$	B_0
Cd	0.3684	14.7	9.5	6.3	11.3	39.1
Te	0.6316	30.5	19.9	11.8	23.4	32.4
CdTe	1	45.2,53.5[a]	29.4,36.5[a]	18.1,19.9[a]	34.7	34.5

[a]Ref. [37]

Table 2: Calculated local and bulk elastic constants of the zinc blende phase of CdTe. Units in GPa. f stands for the fractional occupation.

the (E,V_{Cd}) and (E,V_{Te}) curves can be readily plotted (see Fig. 5). It is now easy to evaluate local atomic-like pressures from these curves using the following definitions formally equivalent to the thermodynamic pressure [16]:

$$p_{\mathrm{Cd}} = -\left(\frac{\partial E}{\partial V_{\mathrm{Cd}}}\right)_T, \quad p_{\mathrm{Te}} = -\left(\frac{\partial E}{\partial V_{\mathrm{Te}}}\right)_T. \tag{7}$$

These equations provide information on the volume reduction of the atomic constituents of the system for a given increase in the crytal energy due to pressure. The higher the atomic pressure, the lower the volume reduction of the corresponding atom. Thus, p_i can be seen as the resistance of the i-th atom to reduce the finite volume that it occupies in the unit cell according to the AIM topological formalism. It becomes interesting to compare the contribution that Cd and Te present in the CdTe polymorphs examined in this work. A plot of the p_{Cd} and p_{Te} values corresponding to different pressures for all the CdTe polymorphs is displayed in Fig. 6 (left). Alternately, $\frac{1}{p_i}$ represents another illustrative microscopic property, that we call atomic mechanical conductance, and is related to the easiness of an atom to reduce its volume when pressure is applied. Obviously, it contains microscopic information that is analogous to the local pressure. It is plotted in Fig. 6

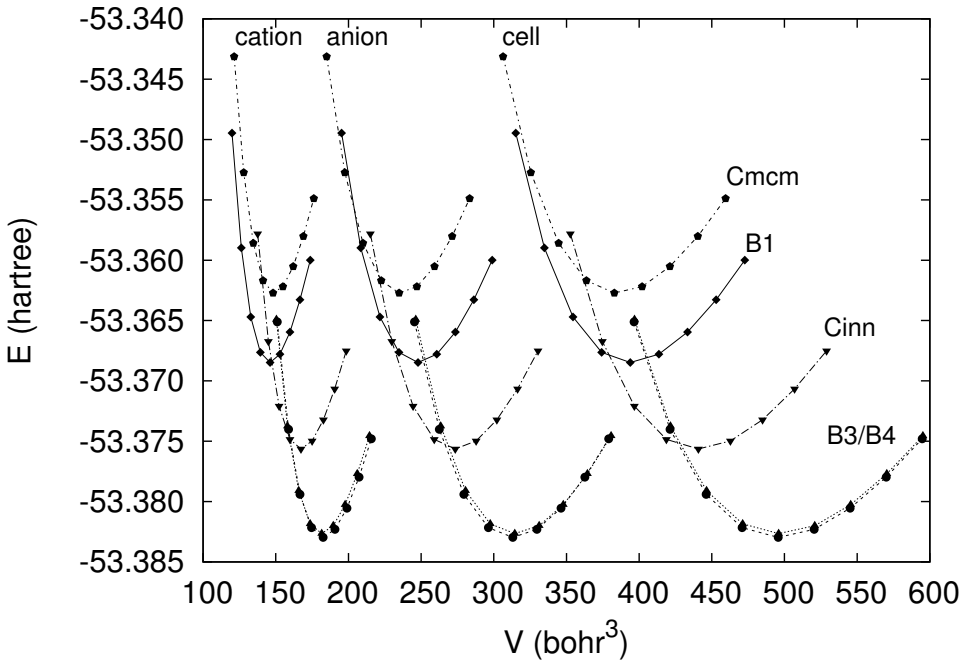

Figure 5: Calculated total energy *versus* atomic and bulk volumes for several CdTe polymorphs. Symbols correspond to the same phases as in Fig. 1.

(right). After a simple manipulation of Eqs. 7, we arrive at $\frac{1}{p}=\frac{1}{p_{\rm Cd}}+\frac{1}{p_{\rm Te}}$, which resembles the equation for a circuit of parallel resistors, p_i playing here the role of a mechanical resistor in agreement with our description above (see Ref. [16] for a thorough discussion of this analogy).

In Fig. 6, we have also represented the corresponding values from our previous calculations in some ZnX (X: S, Se, Te) polymorphs [16]. Several results need to be clarified. Cd behaves as a cation and is clearly more resistant than Te, the anion, as pressure is applied (Fig. 6 (left)). It is apparent that straight lines can nicely connect the thermodynamic pressure (p) with the atomic pressure of Cd ($p_{\rm Cd}$) and Te ($p_{\rm Te}$). The slopes clearly demon-

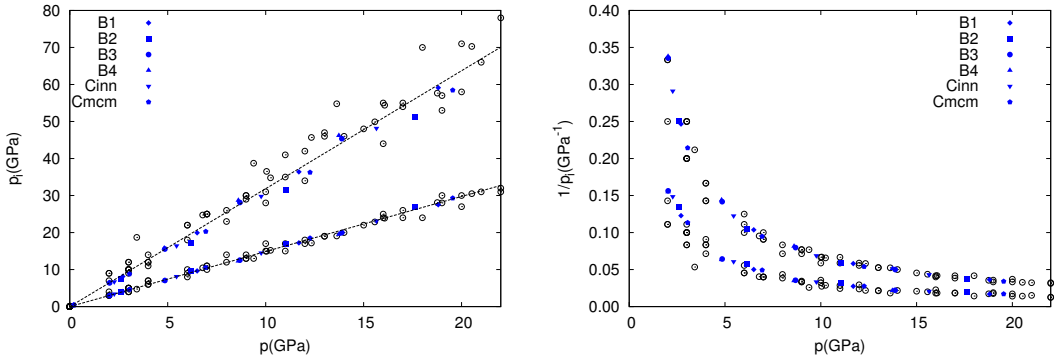

Figure 6: Calculated atomic pressures (left) and mechanical conductances (right) of Cd and Te, and comparison with the corresponding local properties of Zn and X (X: S, Se, Te) in CdTe (this work, solid symbols) and ZnX (Ref. [16], empty symbols) polymorphs.

strate the different mechanical resistances of both atoms, around 3.4 for Cd and 1.4 for Te. As far as similarities are concerned, the lower the pressure, the greater ability to reduce their volume both atoms show (Fig. 6 (right)). We notice that all of these results are independent of the polymorph considered. Perhaps the most important conclusion from these plots is the fact that not only all the points can be grouped in two very well defined curves, one associated with Cd and one with Te, but that this behavior continues even if we consider the calculated local pressures of the other binary chalcogenides (ZnS, ZnSe, ZnTe) investigated in our previous work [16]. This regularity calls for universal trends under pressure for all these semiconductors that can be extended to other families. In fact, this kind of universal behavior has been detected, for example, in the zinc blende-rock salt transition path of several II-VI, III-V and IV-IV compounds [38]. It should be understood that the similar mismatch between the local pressures of the metal and non-metal elements of the semiconductors examined here leads to a similar behavior

regarding the transition mechanism.

3.2.2. Atomic contributions to compressibility and elastic constants

Local compressibility associated with Cd and Te can be defined equivalently to the compressibility of the whole crystal:

$$\kappa = \frac{1}{B_0} = -\frac{1}{V}\left(\frac{\partial V}{\partial p}\right)_T . \tag{8}$$

Taking into account the partition of the cell volume into atomic contributions,

$$V = V_{\mathrm{Cd}} + V_{\mathrm{Te}}, \tag{9}$$

Eq. 8 becomes:

$$\kappa = f_{\mathrm{Cd}}\kappa_{\mathrm{Cd}} + f_{\mathrm{Te}}\kappa_{\mathrm{Te}} \qquad \text{and} \qquad \frac{1}{B_0} = f_{\mathrm{Cd}}\frac{1}{B_{0,\mathrm{Cd}}} + f_{\mathrm{Te}}\frac{1}{B_{0,\mathrm{Te}}} \tag{10}$$

where $f_{\mathrm{Cd}} = V_{\mathrm{Cd}}/V$ and $f_{\mathrm{Te}} = V_{\mathrm{Te}}/V$ are the occupation fractions of Cd and Te, respectively, in the cell, and

$$\kappa_{\mathrm{Cd}} = \frac{1}{B_{0,\mathrm{Cd}}} = -\frac{1}{V_{\mathrm{Cd}}}\left(\frac{\partial V_{\mathrm{Cd}}}{\partial p}\right)_T , \kappa_{\mathrm{Te}} = \frac{1}{B_{0,\mathrm{Te}}} = -\frac{1}{V_{\mathrm{Te}}}\left(\frac{\partial V_{\mathrm{Te}}}{\partial p}\right)_T . \tag{11}$$

Therefore the bulk compressibility results from averaging the local compressibilities in such a way that the contribution from a given atom is proportional to the volume fraction occupied by the atom in the crystal [12]. From these data we can illustrate how the bulk and local compressibilities evolve along the polymorphic sequence (see Fig. 7). The comparison with previous calculated data on ZnX (X: S, Se, Te) polymorhs [16] allows us to notice that the same trend is observed for CdTe, with the cation (Cd or Zn) less compressible than the anion (S, Se or Te) for each compound and polymorph.

However, we observe that the same anion (Te) or the same cation (Zn) shows compressibilities that depends on both the polymorph and the compound. It is not possible to group, as we did above with the local pressure, cations and anions in well–defined and separate universal behaviors if we use local compressibilities.

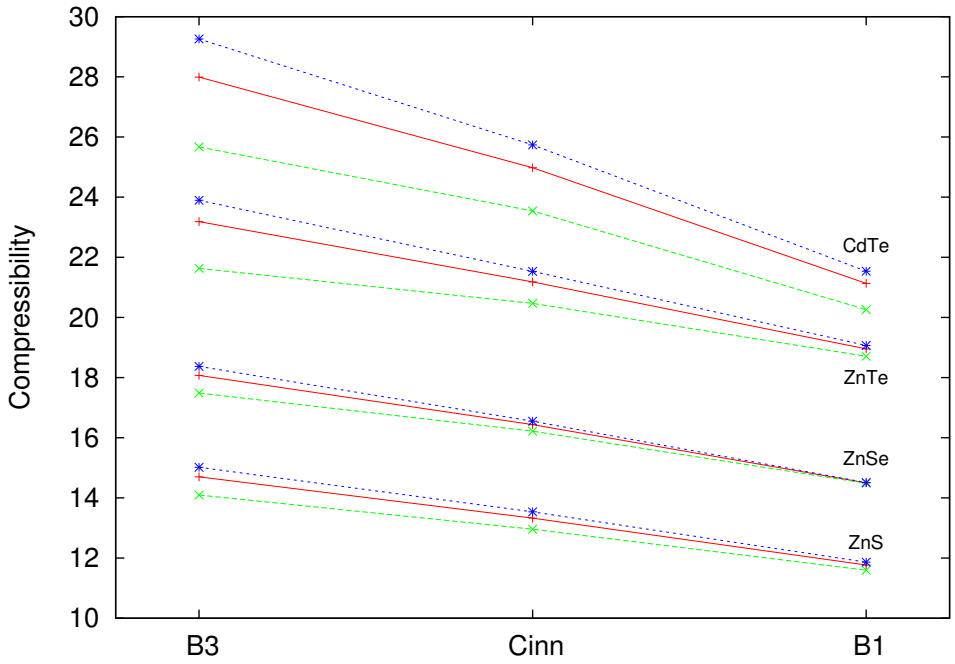

Figure 7: Calculated atomic and bulk compressibilities for several polymorphs of CdTe (this work) and ZnX (X: S, Se, Te) (Ref. [16]). Phases are ordered according to the pressure-induced polymorphic sequence. Stars, pluses and crosses stand, respectively, for the anion (Te, Se, S), the bulk, and the cation (Cd, Zn). Units in 10^2 GPa^{-1}.

Finally, we proceeded to the partition of elastic constants following a similar strategy as the one used to calculate local compressibilities. That is,

combining Eqs. 4 and 9:

$$c_{ij} = \frac{\partial \tau_i}{\partial V} \left[\frac{\partial V_{\mathrm{Cd}}}{\partial \varepsilon_j} \frac{\partial V_{\mathrm{Te}}}{\partial \varepsilon_j} \right] = c_{ij}^{\mathrm{Cd}} + c_{ij}^{\mathrm{Te}}, \tag{12}$$

with c_{ij}^{Cd} being:

$$c_{ij}^{\mathrm{Cd}} = \left[\left(\frac{\partial V_{\mathrm{Cd}}}{\partial \varepsilon_j} \right) \left(\frac{\partial V}{\partial \tau_i} \right)^{-1} \right]_{\varepsilon',0}, \tag{13}$$

with an equivalent definition for c_{ij}^{Te}. Notice that in this case no fractional occupancies are explicitly involved in these equations since they are subsumed in the partial derivatives.

We have computed the stress components, τ_i, for the same values of ϵ_1, ϵ_2, and ϵ_4 as the ones in the calculation of the elastic constants. Two types of fittings were required. First, a low degree polynomial has been used to describe how the unit cell volume changes with the stress components. Second, a low degree polynomial was fitted to the atomic volumes. This way, the necessary derivatives in Eq. 13 are obtained. Table 2 lists the calculated (hypothetical) atomic-like elastic constants for both Cd and Te ions.

The first conclusion that can be drawn from the microscopic elastic constants is that our topological partition is complete in the sense that all c_{ij} are accurately reproduced as a sum of the two atomic contributions. As before, this is a very satisfactory result since the fitting procedures and the computational schemes to evaluate the local contributions and the bulk values of the components of the elasticity tensor are independent. As a result, the bulk modulus of the crystal is recovered by summing up the contributions from each ion (see column $B_{0,\mathrm{el}}$ in Table 2). The definition of the local bulk modulus (last column of Table 2) as the inverse of the local compressibility

does not contain the atomic occupation fraction and can not be compared with the values obtained from the elastic constants. In fact, this column agrees with the chemical intuition of greater bulk modulus associated with the cation in comparison with the bulk modulus of the anion. The results coming from the partition of the elastic constants provides the opposite result: the anion is the one with greater values. It should be noticed that the expressions used to derive these values involve other factors, as the change in the total cell volume with the applied stress, that prevent these microscopic quantities from being considered as purely atomic. The topological partition is not unique, but there are at least two equally well-defined forms that show different behaviors and properties. Furthermore, both partitions complement each other, i.e. from the partition of the compressibility the most and least compressible ions are identified, while by using the partition of the elastic constants the ion that contribute the most to the bulk modulus is found, as fractional occupancies are already subsumed in their operative definition.

4. Summary and conclusions

The response of CdTe to hydrostatic pressure has been investigated by means of first-principles methodologies. Equilibrium geometries, equation of state parameters, and pressure ranges of thermodynamic stabilities have been computed in fair agreement with available experimental data and previous theoretical results. The polymorphic B3 $\rightarrow$ Cinn $\rightarrow$ B1 $\rightarrow$ *Cmcm* $\rightarrow$ B2 sequence has been obtained, thus predicting an eight-fold coordination for Cd and Te at pressures above 70 GPa. This hypothetical B2 phase was confirmed to be fully dynamically stable at pressures above 100 GPa. The

calculation of the elastic constants of the B3 phase of CdTe provides results that confirm the reliability of our computational procedures and allows for the extension of our microscopic analysis of these observable properties.

One important conclusion of the paper is that in fact we can define atomic-like pressures, compressibilities and local elastic constants without having the total energy partitioned into local contributions, thus avoiding a not unequivocal definition and calculation of local energies. Compressibility and elastic constant partitions provide information on atomic contributions to these properties and identify the cation (Cd) as the most difficult crystalline consituent to compress. A general universal behavior is only found when the local pressure concept is invoked. We have seen that all the cations and anions follow well separated linear trends when their calculated local pressures are plotted *versus* hydrostatic pressure for a number of pressure-induced polymorphs of binary II-VI compounds. This result contributes to the understanding of an unified picture for the transition path between the zinc blende and rock salt phases of binary semiconductors [38].

Acknowledgments

Financial and computational support from the MALTA-Consolider Ingenio-2010 program under project CSD2007-00045 is acknowledged. RF, JMM, MM and JMR thanks the Principado de Asturias FICYT agency and Spanish MINECO for financial support (SV-PA-13-ECOEMP-12 and CTQ2012-38599-C02, respectively).

References

[1] A. Bosio, N. Romeo, S. Mazzamuto, V. Canevari, Progress in Crystal Growth and Characterization of Materials 52 (2006) 247.

[2] X. Wu, J.C. Keane, R.G. Dhere, C. Dehert, D.S. Albin, A. Dude, T. A. Gessert, S. Asher, D.H. Levi, P. Sheldon, in: Proceedings of the 17th European Photovoltaic Solar Energy Conference, Munich, Germany, vol. II, 2001, p. 995.

[3] K. Arora, D. U. Bartholomew, D. L. Peterson, A. K. Ramdas, Phys. Rev. B 35 (1987) 7966.

[4] D. Errandonea, A. Segura, D. Martínez-García, V. Mu noz San Jose, Phys. Rev. B 79 (2009) 125203.

[5] A. Mújica, A. Rubio, A. Muñoz, R. Needs, Rev. Mod. Phys. 75 (2003) 863.

[6] R. J. Nelmes, M. I. McMahon, N. G. Wright, D. R. Allan, Phys. Rev. Lett. 73 (1994) 1805.

[7] D. Martínez-García, Y. Le Godec, M. Mézouar, G. Syfosse, J. P. Itié, J. M. Besson, physica status solidi (b) 211 (1999) 461.

[8] M. Côté, O. Zakharov, A. Rubio, M.L. Cohen, Phys. Rev. B 55 (1997) 13025.

[9] I. Lukacevic, D. Kirin, Croat. Chem. Acta 83 (2010) 10.

[10] S. Biering and P. Schwerdtfeger, J. Chem. Phys. 137 (2012) 034705.

[11] J. Contreras-García, P. Mori-Sánchez, B. Silvi, J. M. Recio, J. Chem. Theory Comput. 5 (2009) 2108.

[12] A. Martín Pendás, A. Costales, M. A. Blanco, J. M. Recio, V. Luaña, Phys. Rev. B 62 (2000) 13970.

[13] J. M. Recio, R. Franco, A. Martín Pendás, M. A. Blanco, L. Pueyo, R. Pandey, Phys. Rev. B 63 (2001) 184101.

[14] R. F. W. Bader, Atoms in Moleculess, A Quantum Theory, Oxford, University Press: Oxford, 1990.

[15] A. Otero-de-la-Roza, V. Luaña, J. Phys. Chem. A 115 (2011) 12953.

[16] T. Ouahrani, J. M. Menendez, M. Marqués, J. Contreras-García, V. G. Baonza, J. M. Recio, EPL 98 (2012) 56002.

[17] A brief introduction to the ABINIT software package. X. Gonze, G.-M. Rignanese, M. Verstraete, J.-M. Beuken, Y. Pouillon, R. Caracas, F. Jollet, M. Torrent, G. Zerah, M. Mikami, Ph. Ghosez, M. Veithen, J.-Y. Raty, V. Olevano, F. Bruneval, L. Reining, R. Godby, G. Onida, D.R. Hamann, D.C. Allan, Z. Kristallogr. 220, (2005) 558.

[18] J. P. Perdew, K. Burke, M. Ernzerhof, Phys. Rev. Lett. 77 (1996) 3865.

[19] N. Troullier, J. L. Martins, Phys. Rev. B 43 (2001) 1993.

[20] H. J. Monkhorst, J. D. Pack, Phys. Rev. B 13 (1976) 5188.

[21] M. A. Blanco, E. Francisco, V. Luaña, Comput. Phys. Commun. 158 (2004) 57.

[22] G. V. Sin'ko, N. A. Smirnov, J. Phys.: Condens. Matter 14, (2002) 6989.

[23] Y. Le Page, P. Saxe, Phys. Rev. B 65, (2002) 104104.

[24] L. G. Hector Jr., J. F. Herbst, J. Phys.: Condens. Matt. 20 (2008) 064229.

[25] L. G. Hector Jr., J. F. Herbst, Phys. Rev. B 76 (2007) 014121.

[26] S. Shang, L. G. Hector, Jr., S. Shi, Y. Qi, Y. Wang, Z. Liu, Acta Materialia 60 (2012) 5204.

[27] L. G. Hector Jr., J. F. Herbs, J. Alloys and Compd. 379 (2004) 41.

[28] J. F. Nye, Physical Properties of Crystals, Oxford University Press, Oxford, (1985) p 444.

[29] A. Otero-de-la-Roza, M. A. Blanco, A. Martín Pendás, V. Luaña, Comput. Phys. Commun. 180 (2009) 157.

[30] II-VI and I-VII Compounds; Semimagnetic Compounds, Springer-Verlag, Berlin Heidelberg, (1999) p 1-3.

[31] S. Kumar, M. Ade, T. Nann, Chem. Eur. J. 11 (2005) 2220.

[32] P. Golfinger and M. Jeunehomme, Trans. Faraday Soc. 59 (1963) 2851.

[33] P. Y. Yu, M. Cardona, Fundamentals of Semiconductors, Physics and Materials Properties, Springer-Verlag, Berlin, 2001.

[34] M. Flórez, J. Contreras-García, J. M. Recio, M. Marqués, Phys. Rev. B 79 (2009) 104101.

[35] J. Wrobel, L.G. Hector Jr., W. Wolf, S.L. Shang, Z.K. Liu, K.J. Kurzydlowski, J. Alloys and Compd. 512 (2012) 296.

[36] A. Otero-de-la-Roza, V. Luaña, Phys. Rev. B 84 (2011) 184103.

[37] H.J. McSkimm, D.G. Thomas, J. Appl. Phys. 33 (1962) 56.

[38] M. S. Miao and W. R. L. Lambrecht, Phys. Rev. Lett. 94 (2005) 225501.